ORIGINAL PAPER

CUMULATIVE IMPACT OF VISCOUS DISSIPATION AND HEAT GENERATION ON MHD DARCY-FORCHHEIMER FLOW BETWEEN TWO STRETCHABLE DISKS: QUASI LINEARIZATION TECHNIQUE

SHAHEEN AKHTER[1,2], SOHAIL AHMAD[2]*, MUHAMMAD ASHRAF[2]

Manuscript received: 03.11.2021; Accepted paper: 12.02.2022;
Published online: 30.03.2022.

Abstract. *This research describes the irreversibility analysis of steady flow with magnetic effects between two infinite stretching disks situated in a Darcy-Forchheimer medium. The energy equation is amended by the features of thermal radiation and heat absorption or generation. Similarity transformations are employed to transform the formulated equations into dimensionless form. Quasi linearization technique with the application of mathematical computational software MATLAB is used to acquire the numerical solution of these non-dimensional modeled equations. It is noticed that Eckert number, heat generation/absorption and Forchheimer parameter accelerate the temperature, while the radiation parameter decreases the temperature. It can also be observed that axial velocity is affected by inertia as well as porosity of the medium. Moreover, skin friction coefficient is an escalating function of porosity, magnetic and Forchheimer parameters.*

Keywords: *Magnetohydrodynamics; Darcy-Forchheimer flow; heat source/sink; stretching disks; Quasi linearization method.*

1. INTRODUCTION

Many researchers have been taking great interest in the study of flows between disks due to its practical as well as theoretical aspects. The disk structured bodies are relatively popular in rotating heat exchanger, disk reactors for the production of bio fluids, turbine engines, magnetic storage systems, rotating wafers in the manufacturing process of semiconductor, automobile industries, marine and electronic devices with rotary parts. Also, due to the significant advancement in aeronautical science, the topic of fluid flows between the disks induced by the stretching boundary is of great interest to scientists. The phenomena of stretching flows have a wide range of technical and industrial applications including aircraft engines, drawing of metal films, hydraulic press, metal formation, condensers, rotor-stator system, boilers, and polymer extrusion etc. Due to such numerous applications, many researchers have investigated the fluid flows between the disks induced by the stretching boundaries. Vishwanath et al. [1] used the homotopy analysis method as well as the Computer Extended Series Solution to provide a semi-analytical solution (series solution) to the problem of fluid flow between stretchable disks. Numerical solution of hydrodynamic convective flow over stretchable rotating disks situated in a porous medium has been determined by Gowthami et al. [2]. They used the shooting method along with Newton's method and fourth

[1] COMSATS University (Islamabad), Department of Mathematics, 57000 Sahiwal, Pakistan.
E-mail: shaheen@cuisahiwal.edu.pk.
[2] Bahauddin Zakariya University Multan, Center for Advanced Studies in Pure and Applied Mathematics (CASPAM), 60000 Multan, Pakistan. E-mail: muhammadashraf@bzu.edu.pk.
* *Corresponding author:* sohailkhan1058@gmail.com.

order RK method to solve the nonlinear differential equation. Khan et al. [3] discussed the thermal and mass transfer effects of polymeric fluid flow with in two stretching disks. The numerical solution of non-Newtonian (Maxwell) nanofluid flow with magnetic effects with in two parallel rotating disks was explored by Ahmadian et al. [4]. Hayat et al. [5] analytically examined the flow behavior within two stretching disks situated in a porous medium. They applied the theory of Cattaneo-Christov heat flux to construct the thermal equation. Thermal aspects of a Reiner-Rivlin fluid over the surface of stretchable disk were presented by Rashid and Mustafa [6]. Hafeez et al. [7] numerically analyzed the Souret-Duffor effects on Oldroyd-B fluid flow over a rotating disk. A series solution of the thermal characteristics of laminar and steady stagnation point flow of Reiner-Rivlin fluid was presented by Abhijit Das and B Sahoo [8]. Flow was generated by stretching and rotating the disk in a radial direction. Akhter and Ashraf [9] numerically investigated the fluid flow between stretchable disks. Further studies related to this topic with several flow assumptions can be seen in literature [10-19].

The study of heat transfer plays a significant role in the progress of science and technology. Heat transfer analysis has numerous uses in the polymer industry and several manufacturing processes, such as artificial fibers, micro-electro-mechanical systems, metal extrusion, glass blowing, metal spinning, compact heat exchangers and laser coolant lines etc. Also, analysis of fluid flow via radiative effects has various applications in chemistry, biology, physics and engineering fields involving nuclear reactors, power generation systems, controlling heat factors in high temperature plasma, space and satellites vehicles etc. Whereas, magnetic field effects have significant applications such as pumps, magneto hydrodynamic generators etc. Moreover, the effect of viscous dissipation is quite negligible, but when the fluid viscosity is extremely high, its contribution becomes significant. It affects heat transfer rates and temperature distributions by acting as an energy source. The radiation, magnetic as well as viscous dissipation effects on various flow problems were investigated by several researchers. Hayat et al. [20] analytically examined the effects of magnetohydrodynamic, viscous dissipation and thermal radiation over the fluid flow between coaxial rotating disks. Mustafa Turkyilmazoglua [21] studied the unsteady fluid flow with thermal characteristics caused by vertical motion and rotation of the disk. MHD Casson fluid flow with radiative effects and activation energy over stretching surface was numerically inspected by Zahir et al. [22]. Yu-Ming et al. [23] numerically investigated the radiative heat flow over stretchable surface. The impacts of viscous dissipation, Joule heating and Ohmic dissipation over flow induced by stretched disks were reported numerically by Hashmi et al. [24]. Al-Mdallal et al. [25] used the shooting method to numerically investigate the effects of thermal radiation over Ree-Eyring fluid flow between spinning disks. The effects of joule heating, viscous dissipation, radiation and entropy generation on fluid flow induced by rotating disk were explored by Hayat et al. [26]. Further studies regarding several fluid flows involving different effects can be seen in [27-32].

Nayek et al. [33] examined the physical aspect of thermal radiation on non-porous medium flow induced by rotating the disk. Flow and thermal analysis with the effect of viscous dissipation on Darcy-Forchheimer flow induced by rotating disk was inspected by Hayat et al. [34]. Riasat et al. [35] studied numerically the hydromagnetic effects in 3D squeezing Darcy-Forchheimer flow amid two rotating disks by employing the bvp4c technique. Another interesting contribution on Darcy-Forchheimer flow with viscous dissipation effects was given by Zahir et al. [36]. The homotopy analysis method and shooting technique were applied to solve the modeled problem. Ullah et al. [37] numerically investigated the Darcy-Forchheimer flow induced by rotating the disk. The effects of heat generation/absorption on flow and partial slip effects on the surface of the disk were examined by them. Similar studies with convective heat and mass conditions were performed

by Hayat et al. [38]. More studies regarding Darcy-Forchheimer flow with various flow assumptions can be seen in [39-42].

In light of the aforementioned literature review, the objective of the current study is to present the problem of fluid flow between two infinite stretching disks. To the best of our knowledge and in light of the preceding literature review, it is observed that the current scrutiny has not yet been explored and is being reported for the first time in the literature. An incompressible fluid characterized by the relation of Darcy-Forchheimer is taken between the disks. Moreover, the characteristics of viscous dissipation, heat generation/absorption, thermal radiation and magnetic fields are also examined. Numerical solution is obtained by employing the Quasi linearization technique. The influences of numerous involved parameters on temperature, Nusselt number, skin friction coefficient and velocity are analyzed.

Phenomena of fluid flow through porous media are employed in environmental and industrial systems including heat exchanger design, fibrous insulation, warm protection designing, petroleum technology, geophysics, atomic waste storehouses, catalytic reactors, atomic waste archive, nuclear based repositories, coal combustors, and geothermal energy. The classical Darcy's law is limited to flows of low velocities and weaker porosity. However, many practical processes occur with non-uniformity in porosity and at higher flow rates. The non-Darcian porous medium (known as the Darcy-Forchheimer model), which involves the impacts of vorticity diffusion and inertial drag effects, is probably a modification to classical Darcian theory. Fluid flow via Darcy-Forchheimer media has various applications in industrial and mechanical processes including the process of purifying underground water and oil, pipe developments, outlining and several others.

2. MATERIALS AND METHODS

2.1. PROBLEM STATEMENT

The steady and laminar flow of incompressible fluid with heat transfer between two infinite stretching disks is assumed here. The lower disk is positioned at $z_* = -h^*$ and the upper one is situated at $z_* = h^*$ as seen in Figure. 1. The porous medium amongst the two disks is filled by an incompressible fluid. Porous medium is categorized by the Darcy-Forchheimer relation, which resists fluid motion. The disks are uniformly stretched with stretching rates τ_l and τ_u in radial direction. The stretching velocities are proportional to radial coordinate. A uniform magnetic field is applied normal to the flow direction. Moreover, the effects of viscous dissipation, heat generation/absorption and thermal radiation are also presented. Because the magnetic Reynolds number is considered to be minimal, the induced magnetic field may be ignored in comparison to the applied magnetic field. We assume there is no polarization voltage supplied, therefore the electric field is zero. The geometry of the disk flow problem suggests that it is most appropriate to use a cylindrical polar coordinate system. The mathematical form of velocity field $\vec{v} = (\hat{u}, \hat{v}, \hat{w})$ for flow problem can be written as

$$\hat{u} = \hat{u}(\mathrm{r}, \mathrm{z}_*), \quad \hat{v} = 0, \quad \hat{w} = \hat{w}(\mathrm{r}, \mathrm{z}_*) \tag{1}$$

where $\hat{v}$, $\hat{w}$ and $\hat{u}$ are respective velocity components in the axial, transverse and radial directions. The consequences of heat generation/absorption, viscous dissipation prospective

and thermal radiation are also taken in the energy equation to study the thermal effects of flow through Darcy-Forchheimer medium between the two stretching disks.

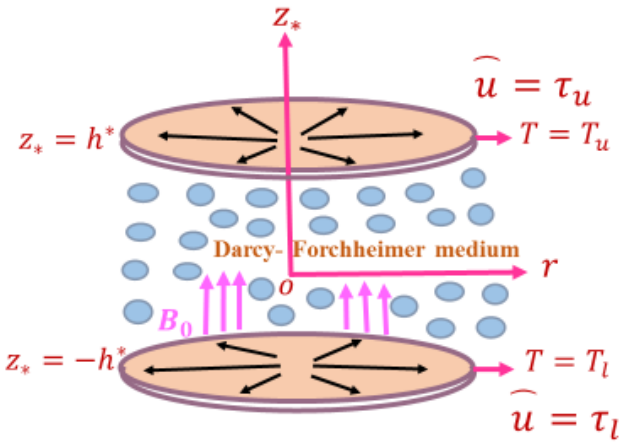

Figure 1. Physical Configuration

Presuming the above flow considerations and followings [9] and [10], the principle equations for present flow problem are summarized as

$$\frac{\hat{u}}{r}+\frac{\partial \hat{u}}{\partial r}+\frac{1}{h^*}\frac{\partial \hat{w}}{\partial \eta}=0, \tag{2}$$

$$\rho_f^*\left(\hat{u}\frac{\partial \hat{u}}{\partial r}+\frac{\hat{w}}{h^*}\frac{\partial \hat{u}}{\partial \eta}\right)-\mu\left(\frac{\partial^2 \hat{u}}{\partial r^2}+\frac{1}{r}\frac{\partial \hat{u}}{\partial r}-\frac{\hat{u}}{r^2}+\frac{1}{h^{*2}}\frac{\partial^2 \hat{u}}{\partial \eta^2}\right)=-\frac{\partial p}{\partial r}+\sigma^* B_0^2\hat{u}-\frac{\mu}{\kappa_p^*}\hat{u}-\frac{\rho_f^* C_b}{\sqrt{\kappa_p^*}}\hat{u}^2, \tag{3}$$

$$\rho_f^*\left(\hat{u}\frac{\partial \hat{w}}{\partial r}+\frac{\hat{w}}{h^*}\frac{\partial \hat{w}}{\partial \eta}\right)-\mu\left(\frac{\partial^2 \hat{w}}{\partial r^2}+\frac{1}{r}\frac{\partial \hat{w}}{\partial r}+\frac{1}{h^{*2}}\frac{\partial^2 \hat{w}}{\partial \eta^2}\right)=-\frac{1}{h^*}\frac{\partial p}{\partial \eta}-\frac{\mu}{\kappa_p^*}\hat{w}-\frac{\rho_f^* C_b}{\sqrt{\kappa_p^*}}\hat{w}^2, \tag{4}$$

$$\rho_f^* c_p\left(\hat{u}\frac{\partial T}{\partial r}+\frac{\hat{w}}{h^*}\frac{\partial T}{\partial \eta}\right)-k_0\left(\frac{1}{h^{*2}}\frac{\partial^2 T}{\partial \eta^2}+\frac{\partial^2 T}{\partial r^2}+\frac{1}{r}\frac{\partial T}{\partial r}\right)-\frac{16\sigma_0 T_u^3}{3k^{\bullet}h^{*2}}\frac{\partial^2 T}{\partial \eta^2}-\frac{\mu}{h^{*2}}\left(\frac{\partial \hat{u}}{\partial \eta}\right)^2-Q_0\left(T-T_u\right)=0. \tag{5}$$

In these equations, μ, η, p, κ_p^*, ρ_f^*, c_p, σ_0, T, $k^{\bullet}$, and k_0 symbolized the dynamic viscosity, similarity variable, the pressure, the Darcy permeability, density of the fluid, the specific heat capacity, Stefan-Boltzmann constant, the temperature, the mean absorption coefficient and the thermal conductivity of the fluid respectively.

Boundary conditions for the flow velocity and temperature distribution at the lower as well as the upper disk are given as,

$$\begin{cases} \hat{u}\left(r,-h^*\right)=r\tau_l, & \hat{u}\left(r,h^*\right)=r\tau_u, \\ \hat{w}\left(r,-h^*\right)=0, & \hat{w}\left(r,h^*\right)=0, \\ T\left(r,-h^*\right)=T_l, & T\left(r,h^*\right)=T_u, \end{cases} \tag{6}$$

(7)

$$\eta=\frac{z_*}{h^*},\quad \hat{u}=-\frac{r\tau_l}{2}g'(\eta),\quad \hat{w}=\tau_l h^* g(\eta),\quad \theta(\eta)=\frac{T-T_u}{T_l-T_u}.$$

By using the similarity variables (7), the partial differential equations (3) - (5) are transformed into ordinary ones. Eqs. (3)-(5) and corresponding boundary conditions (6), in view of Eq. (7), become

$$g'''' - \mathrm{Re}\, gg''' - (M_e\,\mathrm{Re}+\varepsilon)g'' + Fr\,\mathrm{Re}\, g'g'' = 0, \tag{8}$$

$$\left(1+\frac{4}{3}Rd\right)\theta'' - \mathrm{Re}\,\mathrm{Pr}\, g\theta' + \delta\theta + \frac{1}{4}\mathrm{Pr}\, Eng''^2 = 0, \tag{9}$$

$$\left\{\begin{array}{lll} g(-1) = 0, & & g(1) = 0, \\ g'(-1) = -2, & & g'(1) = -2\alpha, \\ \theta(-1) = 1, & & \theta(1) = 0, \end{array}\right\}. \tag{10}$$

Where prime signifies the differentiation w.r.t variable η.

Moreover, $\mathrm{Re}=\frac{\rho_f^*\tau_l h^{*2}}{\mu}$, $M_e=\sqrt{\frac{\sigma^* B_0^2}{\rho\tau_l}}$, $Fr=\frac{C_b r}{\sqrt{\kappa_p^*}}$, $En=\frac{r^2{\tau_l}^2}{\left[c_p(T_l-T_u)\right]}$, $\mathrm{Pr}=\frac{\mu c_p}{k_0}$, $Rd=\frac{4\sigma_0 T_\infty^3}{k^{\bullet} k_0}$, $\delta=\frac{Q_0 h^{*2}}{k_0}$, $\varepsilon=\frac{h^{*2}}{\kappa_p^*}$ and $\alpha=\tau_u/\tau_l$ respectively represent the stretching Reynolds number, the magnetic parameter, Darcy-Forchheimer parameter, the Eckert number, the Prandtl number, the radiation parameter, heat source/sink parameter, the porosity parameter and disk stretching parameter.

2.2. METHODS

The technique of Quasi-linearization is most suitable for transforming the higher order nonlinear equations into linear form. By applying this technique, the numerical solution is attained as follows:

Firstly, the vector sequences $\left\{\hat{g}^{(k)}\right\}$ and $\left\{\hat{\theta}^{(k)}\right\}$ are constructed. Which leads to the numerical solution of Eqs (8) and (9). To construct the sequence $\left\{\hat{g}^{(k)}\right\}$, we linearize the Eq. (8) by keeping only the first order term.

For this purpose, we set

$$\hat{\chi}(g,g',g'',g''',g'''') = Fr\,\mathrm{Re}\, g'g'' - (M_e\,\mathrm{Re}+\varepsilon)g'' - \mathrm{Re}\, gg''' + g'''',$$

which gives rise to:

$$\hat{\chi}\left(\hat{g}^{(k)},\hat{g}'^{(k)},\hat{g}''^{(k)},\hat{g}'''^{(k)},\hat{g}''''^{(k)}\right)+\left(\hat{g}^{(k+1)}-\hat{g}^{(k)}\right)\frac{\partial\hat{\chi}}{\partial\hat{g}^{(k)}}+\left(\hat{g}'^{(k+1)}-\hat{g}'^{(k)}\right)\frac{\partial\hat{\chi}}{\partial\hat{g}'^{(k)}}$$

$$+\left(\hat{g}''^{(k+1)}-\hat{g}''^{(k)}\right)\frac{\partial\hat{\chi}}{\partial\hat{g}''^{(k)}}+\left(\hat{g}'''^{(k+1)}-\hat{g}'''^{(k)}\right)\frac{\partial\hat{\chi}}{\partial\hat{g}'''^{(k)}}+\left(\hat{g}''''^{(k+1)}-\hat{g}''''^{(k)}\right)\frac{\partial\hat{\chi}}{\partial\hat{g}''''^{(k)}}=0.$$

After simplifying, we get the following

$$\begin{aligned}&\hat{g}''''^{(k+1)}+Fr\,\mathrm{Re}\,\hat{g}'^{(k)}\hat{g}''^{(k+1)}-\mathrm{Re}\,\hat{g}^{(k)}\hat{g}'''^{(k+1)}-\varepsilon\hat{g}''^{(k+1)}+Fr\,\mathrm{Re}\,\hat{g}'^{(k)}\hat{g}''^{(k+1)}\\&-M_e\,\mathrm{Re}\,\hat{g}''^{(k+1)}+Fr\,\mathrm{Re}\,\hat{g}''^{(k)}\hat{g}'^{(k+1)}-\mathrm{Re}\,\hat{g}^{(k+1)}\hat{g}'''^{(k)}=Fr\,\mathrm{Re}\,\hat{g}'^{(k)}\hat{g}''^{(k)}-\mathrm{Re}\,\hat{g}^{(k)}\hat{g}'''^{(k)}.\end{aligned}\tag{11}$$

The system of ordinary linear differential equations results from Eq. (11), with $\hat{g}^{(k)}$ symbolizes the solution vector of the k^{th} equation. In order to determine the solution of linear equations, we employ the central difference approximation to discretize the involved derivatives. Which yields the sequence $\left\{\hat{g}^{(k)}\right\}$, which produces the following linear system:

$$L\left(\hat{g}^{(k+1)}\right)=N\ \text{with}\ L\equiv L_{m\times m}\left(\hat{g}^{(k)}\right)\ \text{and}\ N\equiv N_{m\times 1}\left(\hat{g}^{(k)}\right),\tag{12}$$

where, m represents the total number of grid points.

And to construct the sequence $\left\{\hat{\theta}^{(k)}\right\}$, we proceed as follows,

$$\left(1+\frac{4}{3}Rd\right)\hat{\theta}''^{(k+1)}-\mathrm{Re}\,\mathrm{Pr}\,\hat{g}^{(k+1)}\hat{\theta}'^{(k+1)}+\delta\hat{\theta}^{(k+1)}+\frac{1}{4}\mathrm{Pr}\,Ec\hat{g}''^{(k+1)^2}=0.\tag{13}$$

A diagonally dominant system is obtained by employing the central difference approximation, which allows us to use the SOR method.

The computational procedure is summarized as follows:

- An initial guess for $\hat{g}^{(0)}$ and $\hat{\theta}^{(0)}$, is chosen that fulfills the boundary conditions stated in Eq. (10).

- Find the approximation $\hat{g}^{(1)}$, by solving the linear system of Eq. (12).

- Use the approximation $\hat{g}^{(1)}$ to solve the linear system that arises from the finite difference discretization of Eq. (13), to obtain the approximation $\hat{\theta}^{(1)}$.

- Take $\hat{g}^{(1)}$ and $\hat{\theta}^{(1)}$, as new initial guesses. Repeat the procedure to obtain the vector sequences $\left\{\hat{g}^{(k)}\right\}$ and $\left\{\hat{\theta}^{(k)}\right\}$ that converges to the respective numerical solution of Eqs. (8) and (9).

- The vector sequences $\left\{\hat{g}^{(k)}\right\}$ and $\left\{\hat{\theta}^{(k)}\right\}$ are generated till

$$\max\left(\left\|\hat{\theta}^{(k+1)}-\hat{\theta}^{(k)}\right\|_{l\infty},\left\|\hat{g}^{(k+1)}-\hat{g}^{(k)}\right\|_{l\infty}\right)<Tol_{itr}.$$

3. RESULTS AND DISCUSSION

The main concern of the present study is to numerically investigate the flow characteristics of Darcy-Forchheimer fluid flow between two stretchable disks in the presence of applied magnetic field. The graphical and tabular representations of our findings, as well as their interpretations and discussion, are included in this section. The numerical results for shear stresses, heat transfer rate, velocity fields and temperature distributions between the disks are obtained for a wide range of values of Forchheimer parameter *Fr*, porosity parameter ε, magnetic parameter M_e, disk stretching parameter α, heat absorption parameter δ, radiation parameter *Rd*, and Eckert number *En*.

Firstly, the graphical interpretation of our findings is presented here. Streamlines for the current flow problem are depicted in Fig. 2. The streamlines along the walls are obviously quite close to one another, indicating the significant gradients of stream function, yielding the higher fluid velocity nearer to the disks. It is noted from Figure 3a and 3b that the same results are obtained for radial velocity $g'(\eta)$ for disk stretching parameter γ (which is α in the present case) under some certain limiting conditions as were obtained by Khan et al. [10]. It is noticed here that the axial velocity increases with an increase in the disk stretching parameter. The graphical comparison is assessed to be in a good relation with the existing literature.

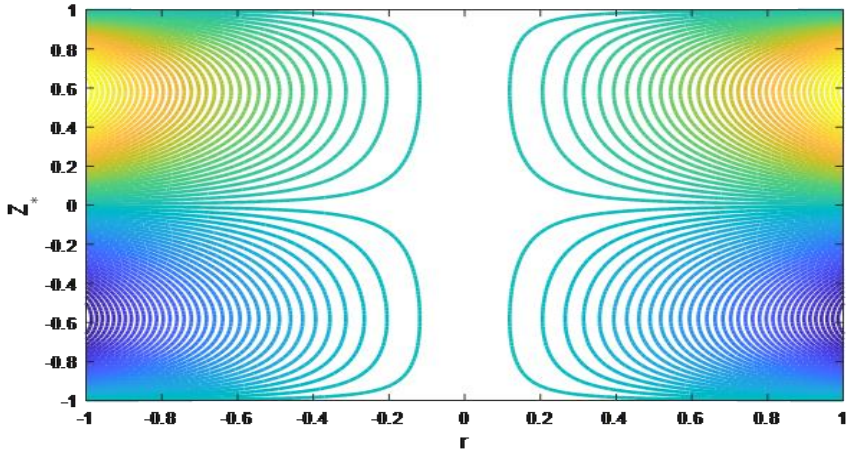

Figure 2. Streamlines for $\alpha = 1$, $Re = 0.5$, $Fr = 0.5$, $En = 0.1$, $\varepsilon = 0.5$, $M_e = 0.5$, $Rd = 1.7$, $\Pr = 1.7$, **and** $\delta = 0.1$

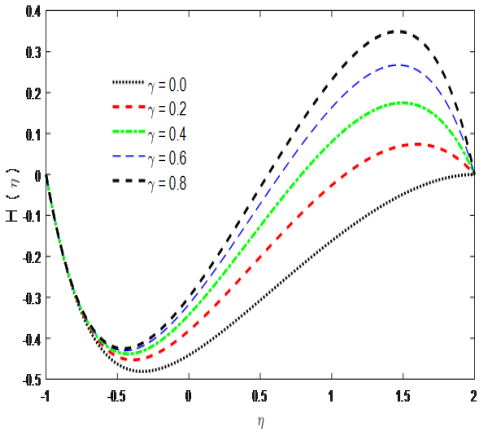

Figure 3a. Present Result

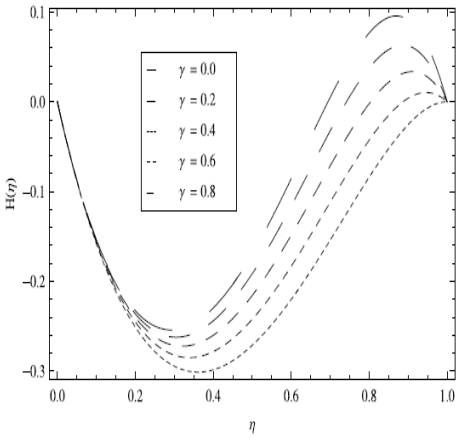

Figure 3b. Comparison with Khan et al. [10] under certain conditions

Figs. 4 and 5 are portrayed to illustrate the variation in axial and radial velocity via magnetic parameter M_e. The axial velocity $g(\eta)$ tends to increase but it's worth noting that radial velocity $g'(\eta)$ has an inversely proportional to Hartmann number. Physically, the flow direction is normal to the applied magnetic field. Drag force known as Lorentz force (having tendency to slow the flow speed) is produced due to the applied magnetic field, which resists the fluid motion. Fig. 6 demonstrates the decreasing trend in temperature profile with magnetic parameter M_e.

The impacts of local inertia or Darcy-Forchheimer parameter on the profiles such as axial velocity $g(\eta)$, radial velocity $g'(\eta)$ and temperature $\theta(\eta)$ are depicted in Figs. 7-9. The axial velocity gets increase near lower disk and decreases near upper disk with the effect of Fr.

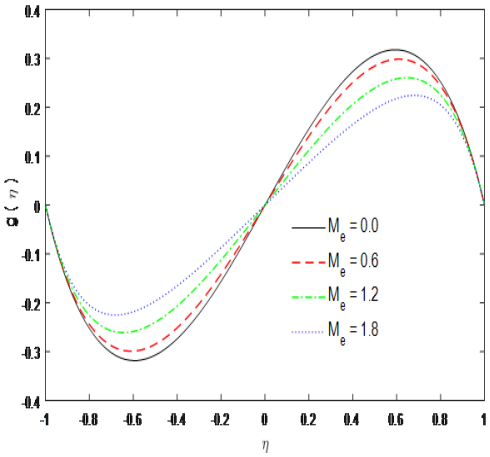

Figure 4. The variation in axial velocity for $\mathrm{Re}=6$, $\varepsilon=2.5$, $\alpha=1$, $En=3.2$, $Rd=1.9$, $\mathrm{Pr}=1.7$, $\delta=0.3$, $Fr=2.5$ **and various** M_e

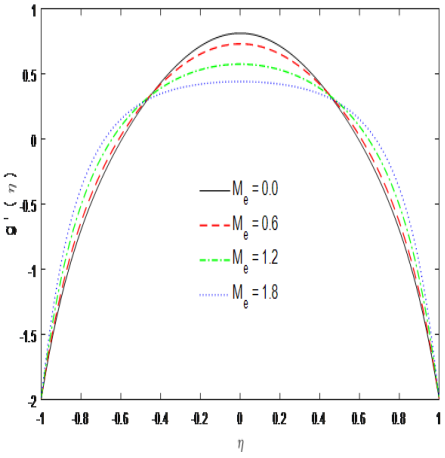

Figure 5. The variation in radial velocity for $\mathrm{Re}=6$, $\varepsilon=2.5$, $\alpha=1$, $En=3.2$, $Rd=1.9$, $\mathrm{Pr}=1.7$, $\delta=0.3$, $Fr=2.5$ **and various** M_e

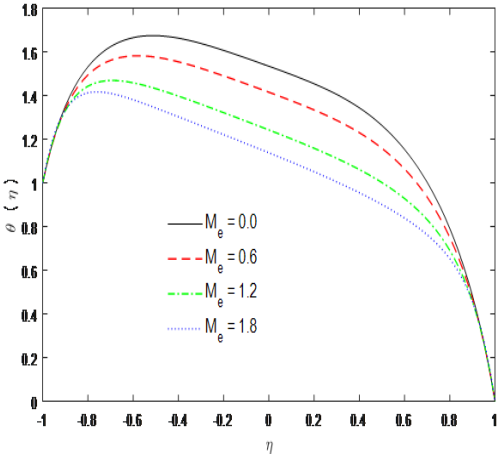

Figure 6. The variation in temperature for $\mathrm{Re}=6$, $\varepsilon=2.5$, $\alpha=1$, $En=3.2$, $Rd=1.9$, $\mathrm{Pr}=1.7$, $\delta=0.3$, $Fr=2.5$ **and various** M_e

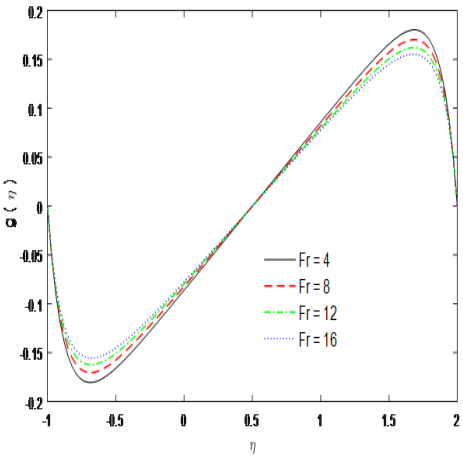

Figure 7. The variation in axial velocity for $\mathrm{Re}=12$, $\varepsilon=3$, $\alpha=1$, $En=3.2$, $Rd=1.2$, $\mathrm{Pr}=1.7$, $\delta=0.2$, $M_e=1.9$, **and various** Fr

On the other side, the radial velocity attains its maximum value near upper disk. Further, local inertia is responsible for an increase in the temperature. The surface drag is proportional to the inertial coefficient or Forchheimer parameter due to which the resistive force increases which causes an enhancement in temperature. Axial velocity upsurges with the

influence of porosity parameter ε (see Fig. 10). But contrarily the radial velocity and temperature downturn with the effect of ε, as shown in Figs. 11 and 12.

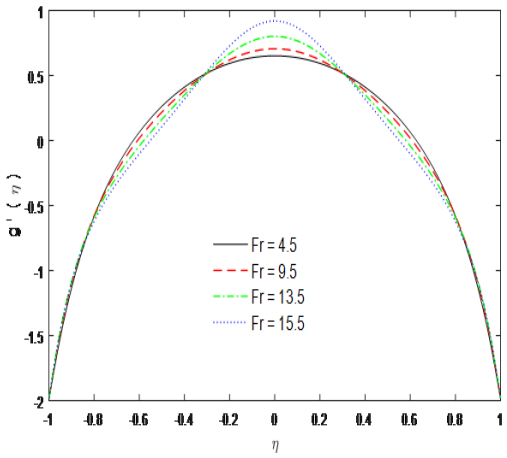

Figure 8. The variation in radial velocity for $M_e = 1.5$, $\mathrm{Re} = 3$, $\varepsilon = 2.8$, $\alpha = 1$, $En = 3.2$, $Rd = 1.2$, $\mathrm{Pr} = 1.7$, $\delta = 0.2$, **and various** Fr

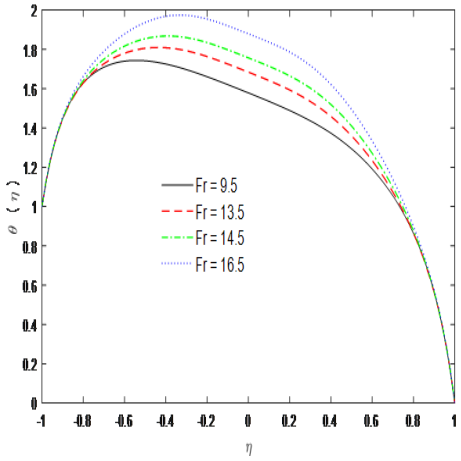

Figure 9. The variation in temperature for $M_e = 1.5$, $\mathrm{Re} = 3$, $\varepsilon = 2.8$, $\alpha = 1$, $En = 3.2$, $Rd = 1.2$, $\mathrm{Pr} = 1.7$, $\delta = 0.2$, **and various** Fr

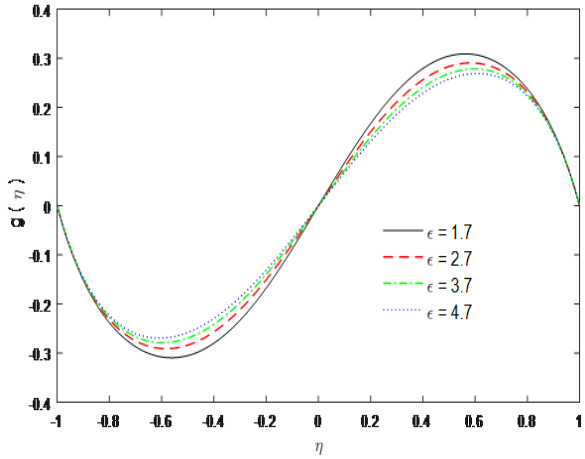

Figure 10. The variation in axial velocity for $M_e = 0.5$, $\mathrm{Re} = 10$, $\alpha = 1$, $En = 3.2$, $Rd = 1.9$, $\mathrm{Pr} = 1.7$, $\delta = 0.3$, $Fr = 3$ **and various** $\mathcal{E}$

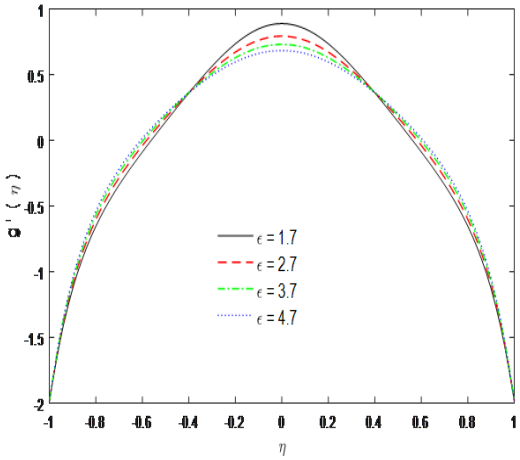

Figure 11. The variation in radial velocity for $M_e = 0.5$, $\mathrm{Re} = 10$, $\mathrm{Pr} = 1.7$, $Rd = 1.9$, $\alpha = 1$, $En = 3.2$, $\delta = 0.3$, $Fr = 3.5$ **and various** $\mathcal{E}$

A decrease in the momentum and velocity layer thickness is associated with the permeable media due to which fluid motion faces resistance. Thus the utilization of permeable media is much eminent to control the flow nature. The consistency in the flow can also be achieved by using porous media. From the outcomes of Figs. 13 and 14, it is revealed that the effect of relative disk stretching parameter is to enhance the both axial and radial velocity of the fluid. The variation in temperature is illustrated in Fig. 15 for distinct Eckert number values. This figure portrays that an enhancement in the values of Eckert number tends to escalate the temperature together with thermal boundary layer thickness. The ratio of the product of the difference between the temperatures of the fluid and the specific heat to the square of the fluid velocity refers to as the Eckert number for which $En = 0$ signifies no viscous dissipation. It is important to mention that fluid motion is desirably controlled by the Eckert number. A viscous force is generated under the action of viscous stress caused by the internal energy, so that; the viscous dissipation ($En < 0$ or $En > 0$) causes an increase in the thermal boundary layer. Fig. 16 elaborates the effects of radiation parameter Rd over

temperature distribution. It is observed that enhancement in radiation parameter Rd causes a decrease in temperature. So, by augmenting the radiation parameter induces the decrease in fluid regime's thermal diffusivity, which is responsible for reducing the heat energy in boundary layer. As a consequence, thermal boundary layer thickness and the fluid's temperature are decreased.

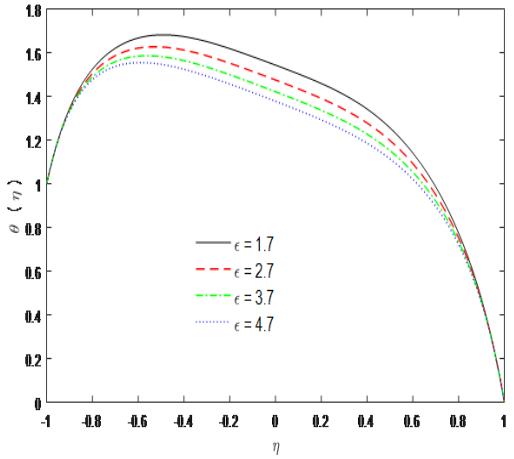

Figure 12. The variation in temperature for $M_e = 0.5$, $\mathrm{Re} = 5$, $Fr = 3.5$, $\alpha = 1$, $En = 3.2$, $Rd = 1.9$, $\mathrm{Pr} = 1.7$, $\delta = 0.3$, **and various** ε

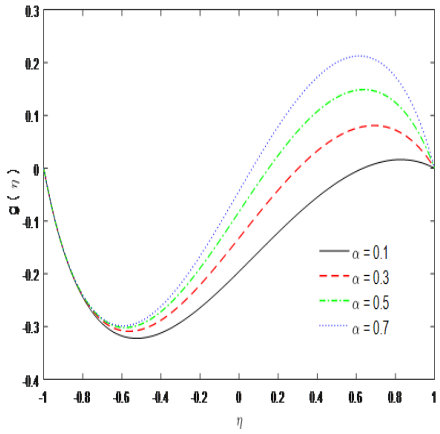

Figure 13. The variation in axial velocity for $M_e = 0.5$, $\mathrm{Re} = 6$, $\varepsilon = 3.5$, $Fr = 3.5$, $En = 3.2$, $Rd = 1.9$, $\mathrm{Pr} = 1.7$, $\delta = 0.3$, **and various** α

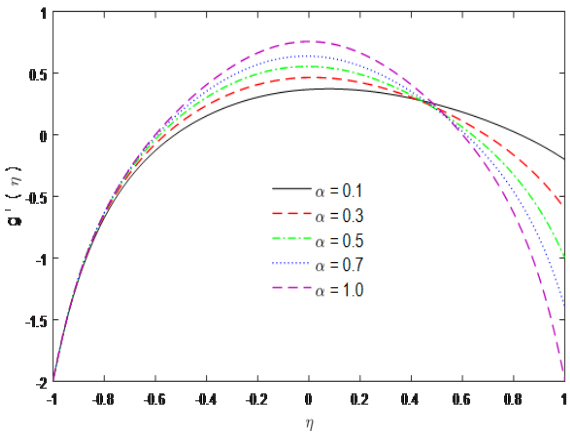

Figure 14. The variation in radial velocity for $M_e = 0.5$, $\mathrm{Re} = 6$, $\varepsilon = 3.5$, $En = 3.2$, $Rd = 1.9$, $\mathrm{Pr} = 1.7$, $\delta = 0.3$, $Fr = 3.5$ **and various** α

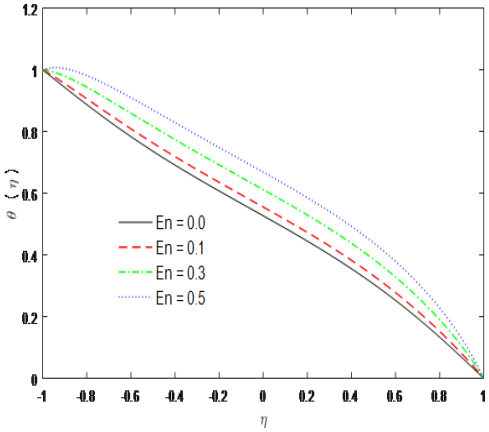

Figure 15. The variation in temperature for $M_e = 0.5$, $\mathrm{Re} = 5$, $\alpha = 1$, $\varepsilon = 3.5$, $Rd = 1.9$, $\mathrm{Pr} = 1.7$, $\delta = 0.3$, $Fr = 3.5$ **and various** En

Figure 17 is plotted to express the variation in temperature profiles with the influence of heat source/sink parameter δ. The presence of δ is responsible for increasing thermal boundary layer thickness as the thermal state of the fluid is improved by augmenting the heat source/sink parameter δ. Physically, a significant amount of heat is introduced into the system by increasing the heat source parameter, causing the fluid temperature to increase.

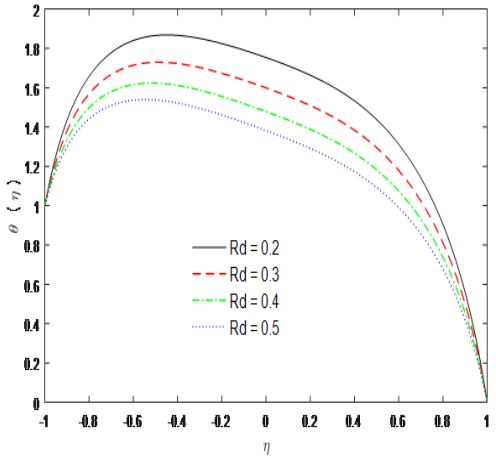

Figure 16. The variation in temperature for $M_e = 0.5,\ \mathrm{Re} = 5,\ Fr = 3.5,\ \alpha = 1,\ En = 3.2,\ \varepsilon = 3.5,\ \mathrm{Pr} = 1.7,\ \delta = 0.3,$ **and various** Rd

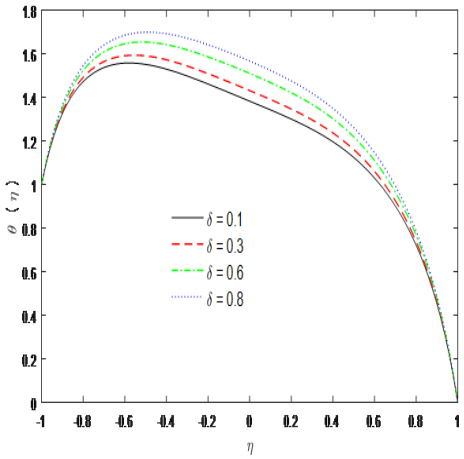

Figure 17. The variation in temperature for $M_e = 0.5,\ \mathrm{Re} = 5,\ \varepsilon = 3.5,\ Fr = 3.5,\ En = 3.2,\ Rd = 1.9,\ \mathrm{Pr} = 1.7,\ \alpha = 1,$ **and various** δ

Table 1. Extrapolated values for $\theta(\eta)$

$\alpha = 1, Re = 6, Fr = 0.5, En = 1.2, \varepsilon = 0.5, M_e = 0.5, Rd = 0.2, \mathrm{Pr} = 0.2, \delta = 0.5$ **with various** η

η	1st grid (η = 0.02)	2nd grid (η = 0.01)	3rd grid (η = 0.005)	Extrapolation values
-0.6	0.99600	0.99617	0.99622	0.99623
-0.2	0.85354	0.85375	0.85380	0.85382
0.0	0.76180	0.76201	0.76207	0.76209
0.2	0.65784	0.65805	0.65811	0.65812
0.6	0.40075	0.40093	0.40098	0.40100

The tabular analysis reveals the impacts of the prime parameters on both lower as well as upper disk. Table 1 exhibits the extrapolation values for temperature $\theta(\eta)$ against several grid sizes η. The values converge in a best way by decreasing the grid sizes which affirm the precision of our code.

Tables 2-4 are provided to check out the impacts of the magnetic, Forchheimer and porosity parameters respectively on shear stresses $g''(\pm 1)$ and heat transport rates $\theta'(\pm 1)$. It is worth noting here that both the shear stresses and the rates of heat transfer substantially elevate with the influence of M_e, Fr and ε. The transfer rates of heat on upper and lower disks are negligibly affected by the Forchheimer and porosity parameters. On the other hand, these parameters have a remarkable effect on both surfaces of disk. The physical reason for this fact is the pores size of the medium. The large voids in a porous medium insert low effect on velocity and Nusselt number as well.

Table 2. Shear stress and heat transfer rate for

$Re = 4, \alpha = 1, En = 1.6, \varepsilon = 1.5, Fr = 0.5, Rd = 1.4, \mathrm{Pr} = 1.7, \delta = 0.3$ **with various** M_e

M_e	$g''(-1)$	$\theta'(-1)$	$g''(1)$	$\theta'(1)$
0.0	7.61114	2.72606	-7.61114	-3.99637
0.5	7.93655	2.73429	-7.93655	-3.99704
1.0	8.81916	2.79468	-8.81916	-4.03796
1.5	10.06627	2.95256	-10.06627	-4.17099
2.0	11.51428	3.20597	-11.51428	-4.39929

Table 3. Shear stress and heat transfer rate for $Re=4,\alpha=1,En=1.6,\varepsilon=1.5,M_e=0.5,Rd=1.4,\Pr=1.7,\delta=0.3$ **with various** Fr

Fr	$g''(-1)$	$\theta'(-1)$	$g''(1)$	$\theta'(1)$
0.2	7.83110	2.73335	-7.83110	-3.99613
0.4	7.90163	2.73393	-7.90163	-3.99668
0.6	7.97123	2.73470	-7.97123	-3.99745
0.8	8.03988	2.73568	-8.03988	-3.99844
1.0	8.10758	2.73685	-8.10758	-3.99965

Table 4. Shear stress and heat transfer rate for $Re=4,Fr=0.5,En=1.6,\alpha=1,M_e=0.5,Rd=1.4,\Pr=1.7,\delta=0.3$ **with various** ε

ε	$g''(-1)$	$\theta'(-1)$	$g''(1)$	$\theta'(1)$
1.2	7.84081	2.73100	-7.84081	-3.99595
1.6	7.96813	2.73553	-7.96813	-3.99755
2.0	8.09278	2.74114	-8.09278	-4.00033
2.4	8.21491	2.74772	-8.21491	-4.00416
2.8	8.33463	2.75517	-8.33463	-4.00894

Table 5 reveals the several heat transfer rates for diverse values of Eckert and Prandtl numbers. The values of Nusselt number are the escalating functions of $\theta'(-1)$ and $\theta'(1)$. The values of En and $\Pr$ are taken in such a way that we may attain the optimal solution. The rates of heat transfer seem to be decrease at lower disk for several values of thermal radiation parameter, as appeared in Table 6. Contrarily, the heat source/sink parameter causes an increment in heat transport rates on both upper and lower disks (see table 6). The values of the physical parameters along with the disk stretching velocity can be adjusted in such a way that we may attain certain factual applications of the concerned work.

Table 5. Shear stress and heat transfer rate for $Re=4,Fr=0.5,\alpha=1,Me=0.5,Rd=1.4,\delta=0.3$ **with various** En and $\Pr$

En	$\theta'(-1)$	$\theta'(1)$	Pr	$\theta'(-1)$	$\theta'(1)$
0.1	-0.35216	-0.91058	0.2	-0.08546	-0.91220
0.3	0.05936	-1.32210	0.4	0.26434	-1.29543
0.5	0.47089	-1.73363	0.6	0.62153	-1.68665
0.7	0.88242	-2.14516	0.8	0.98644	-2.08620
0.9	1.293949	-2.55669	1.0	1.35944	-2.49442

Table 6. Shear stress and heat transfer rate for $Re=4,Fr=0.5,En=1.6,\alpha=1,M_e=0.5,\Pr=1.7,\varepsilon=1.5$ **with various** Rd *and* δ

Rd	$\theta'(-1)$	$\theta'(1)$	δ	$\theta'(-1)$	$\theta'(1)$
0.2	8.49918	-10.15134	0.1	2.62182	-3.90699
0.4	6.39459	-7.91947	0.3	2.73429	-3.99704
0.6	5.10740	-6.54574	0.5	2.85430	-4.09440
0.8	4.23280	-5.60872	0.7	2.98277	-4.20001
1.0	3.59766	-4.92650	0.9	3.12079	-4.31494

4. CONCLUSIONS

An inclusive numerical analysis of a Darcy-Forchheimer steady fluid flow with constant density and viscosity between stretchable disks is offered in this paper. The flow is resisted by a porous medium between the disks. The flow also involves heat transfer attributes under the influences of viscous dissipation, heat source/sink and thermal radiation. A persuasive numerical technique named Quasi-linearization is utilized to attain the numerical solutions of the governing coupled flow model equations. The main culminations of this study may be listed as:

- the axial velocity accelerates near lower disk and decelerates near upper disk with the impact of Forchheimer parameter;
- the parameters such as magnetic, porosity and Forchheimer tend to escalate the shear stresses and rates of heat transport on both disks;
- the magnetic parameter causes an increase in the axial velocity $g(\eta)$ but its effect is to decrease the radial velocity $g'(\eta)$;
- the Eckert number substantially escalates the temperature and thermal boundary layer thickness as well;
- the values of Nusselt numbers are enhanced by the viscous dissipation and reduced by the thermal radiation parameter;
- an enhancement in the radiation parameter causes a decrease in the temperature;
- the effect of relative disk stretching parameter is to enhance the both axial and radial velocity of the fluid.

REFERENCES

[1] Awati, V. B., Jyoti, M., Prasad, K. V., *Engineering Science and Technology, an International Journal*, **20**, 1211, 2017.
[2] Gowthami, K., Prasad, P. H., Mallikarjuna, B., Makinde, O. D., *Songklanakarin Journal of Science and Technology*, **42**, 391, 2020.
[3] Khan, N., Hashmi, M. S., Khan, S. U., Syed, A. W., *Journal of the Brazilian Society of Mechanical Sciences and Engineering*, **40**, 1, 2018.
[4] Ahmadian, A., Bilal, M., Khan, M. A., Asjad, M. I., *Scientific Reports*, **10**, 2020.
[5] Hayat, T., Qayyum, S., Imtiaz, M., Alsaedi, A., *Results in Physics*, **7**, 126, 2017.
[6] Rashid, M. U., Mustafa, M., *Ain Shams Engineering Journal*, **12**, 875, 2021.
[7] Hafeez, A., Khan, M., Ahmed, J., Ahmed, A., Iqbal, Z., *Arabian Journal of Science and Engineering*, **45**, 5949, 2020.
[8] Das, A., Sahoo, B., *Fluid Mechanics Research International Journal*, **2**, 73, 2018.
[9] Akhter, S., Ashraf, M., *Thermal Science*, **25**, 989, 2021.
[10] Khan, N., Sajid, M., Mahmood, T., *AIP Advances*, **5**, 057115, 2015.
[11] Hayat, T., Kainat, Z., Khan, S. A., Alsaedi, A., *Preprints*, 2021030232, 2021.
[12] Abbas, N., Nadeem, S., Saleem, S., Issakhov, A., *Ain Shams Engineering Journal*, 2021.
[13] Awati, V. B., Jyoti, M., Prasad, K. V., *Engineering Science and Technology, an International Journal*, **20**, 1211, 2017.
[14] Guria, M., *International Journal of Applied Mechanics*, **23**, 623, 2018.
[15] Wu, X. S., Luo, Y., Chu, G. W., Xu, Y. C., Sang, L., Sung, B. C., Chen, J. F., *Journal of Industrial and Engineering. Chemistry*, **57**, 7692, 2018.

[16] Bilal, S., Tassaddiq, A., Majeed, A. H., Nisar, K. S., Ali, F., Malik, M. Y., *Frontiers in Physics*, 210072839, 2019.
[17] Zaib, A., Khan, U., Khan, I., Seikh, A. H., Sherif, E. S. M., *Symmetry*, **11**, 1520, 2019.
[18] Hussain, S., Ahmad, F., Shafique, M., *Asia Pacific Journal of Multidisciplinary Research*, **1**, 2013.
[19] Munawar, S., Ali, A., Saleemand N., Naqeeb, A., *Journal of Mechanics*, **30**, 339, 2014.
[20] Hayat, T., Qayyum, S., Imtiaz, M., Alsaedi, A., *PLOS One*, **11**, e0155899, 2016.
[21] Turkyilmazoglua, M., *Physics of Fluids*, **30**, 063605, 2018.
[22] Shah, Z., Kumam, P., Deebani, W., *Scientific Reports*, **10**, 4402, 2020.
[23] Chu, Y. M., Adnan, Khan, U., Ahmed, Naveed, Din, M., Tauseef, S., Khan, I., *Open Physics*, **18**, 842, 2020.
[24] Hashmi, M. S., Khan, N., Khan, S. U., Khan, M. I., Khan, N. B., Nazeer, M., Kadry, S., Chu, Y. M., *Alexendria Engineering Journal*, **60**, 767, 2021.
[25] Mdallal, Q. M. A., Renuka, A., Muthtamilselvan, M., Abdalla, B., *Ain Shams Engineering Journal*, 2021.
[26] Hayat, T., Qayyum, S., Khan, M. I., Alsaedi, A., *Physics of Fluids*, **30**, 017101, 2018.
[27] Ahmed, N., Adnan, Khan, U., Din, S. T. M., *Alexandria Engineering Journal*, **57**, 1893, 2018.
[28] Khan, U., Adnan, Ahmed, N., Din, S. T. M., *The European Physical Journal Plus*, **132**, 166, 2017.
[29] Khan, U., Abbasi, A., Ahmed, N., Din, S.T M., *Engineering Computations*, **34**, 2479, 2017.
[30] Adnan, Khan, U., Ahmed, N., Din, S. T. M., Alharbi, S. O., Khan, I., *Alexandria Engineering Journal*, **61**, 2318-2329, 2022.
[31] Adnan, Khan, U., Ahmed, N., Din, S. T. M., Khan, I., Asad, M. F. A., *Mathematical Problems in Engineering*, **2021**, 3138301, 2021.
[32] Adnan A.S., Khan, S. I. U., Ahmed, N., Din, S. T. M., Khan, I., Nisar, K. S., *Scientific Reports*, **11**, 9837, 2021.
[33] Nayak, M. K., Shaw, S., Khan, M. I., Pandey, V. S., Nazeer, M., *Journal of Materials Research and Technology*, **9**, 7387, 2020.
[34] Hayat, T., Haider, F., Muhammad, T., Alsaedi, A., *Applied. Mathematics and Mechanics, (English Edition)*, **41**, 741, 2020.
[35] Riasat, S., Ramzan, M., Kadry, S., Chu, Y. M., *Scientific Reports*, **10**, 17208, 2020.
[36] Shah, Z., McCash, L. B., Dawar, A., Bonyah, E., *AIP Advances*, **10**, 065137, 2020.
[37] Ullah, M. Z., Capizzano, S. S., Baleanu, D., *Frontiers of Physics*, 2020.
[38] Hayat, T., Aziz, A., Muhammad, T., Alsaedi, A., *International Journal of Numerical Methods for Heat and Fluid Flow*, **28**, 2531, 2018.
[39] Saeed, A., Alghamdi, W., Mukhtar, S., Shah, S. I. A., Kumam, P., Gul, T., Nasir, S., Kumam, W., *PLOS One*, 2021.
[40] Adnan, Khan, U., Ahmed, N., Din, S. T. M., Baleanu, D., Nisar, K. S., Khan, I., *Computers Materials and Continua*, **680**, 213-228, 2021.
[41] Khan, U., Adnan, Ahmed, N., Din, S. T. M., Baleanu, D., Khan, I., Nisar, K. S., *Energies*, 2020, ***13***, 1686, 2020.
[42] Khan, U., Adnan, Ahmed, N., Din, S. T. M., Chu, Y. M., Khan, I., and Nisar, K. S., *Molecules*, ***25***, 1777, 2020.